Supplement of Atmos. Chem. Phys., 26, 8387–8405, 2026
https://doi.org/10.5194/acp-26-8387-2026-supplement

Atmospheric Chemistry and Physics
Open Access

Supplement of

Measurement report: Validation of multi-satellite remote sensing products and potential source apportionment of BrO and IO in the Arctic using ship-based DOAS

Qijin Zhang et al.

Correspondence to: Chengzhi Xing (xingcz@aiofm.ac.cn) and Cheng Liu (chliu81@ustc.edu.cn)

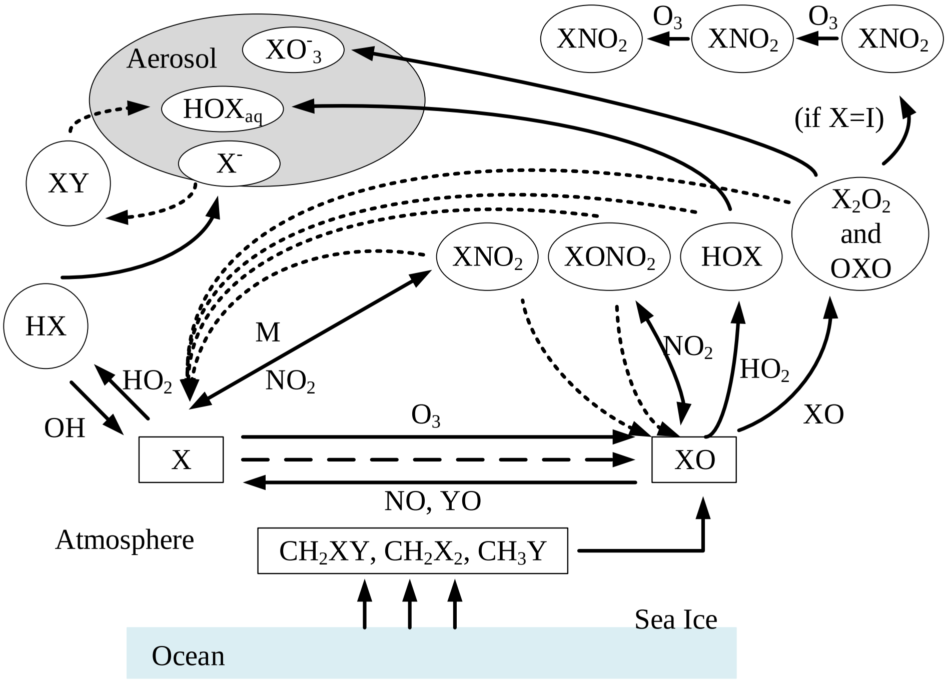

Fig. S1. Simplified chemical diagram of iodine and bromine in the Arctic.

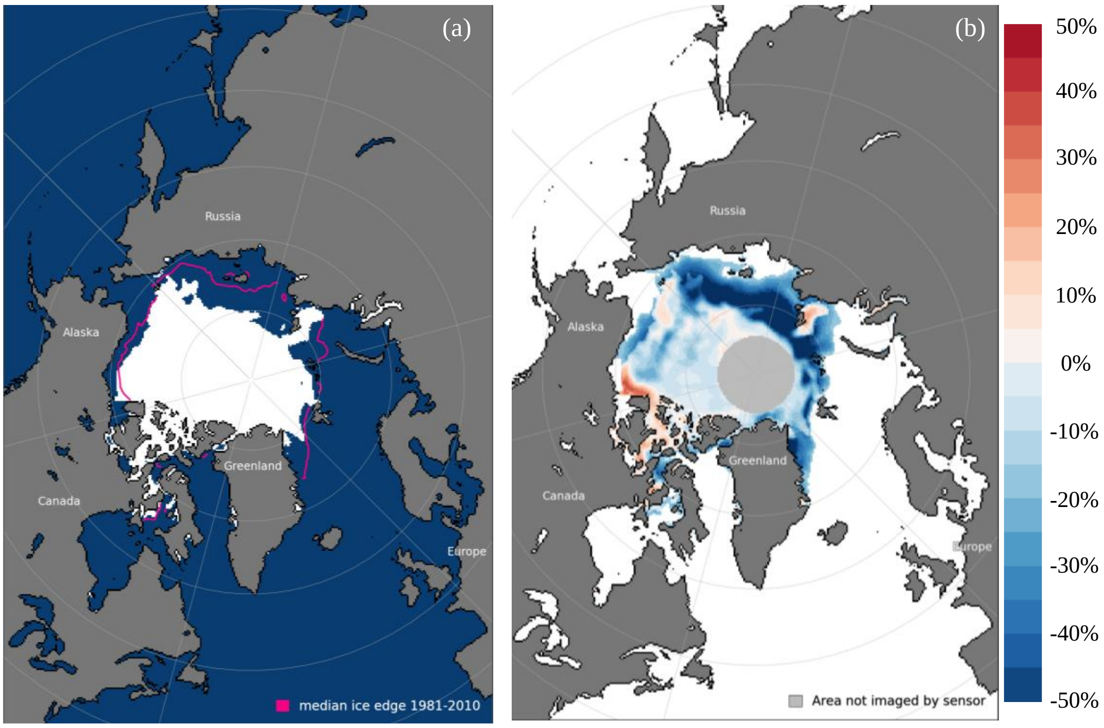

Fig. S2. (a) Arctic sea ice extent (August 2021); (b) Arctic sea-ice concentration.
Data source: http://nsidc.org/data/seaice_index/

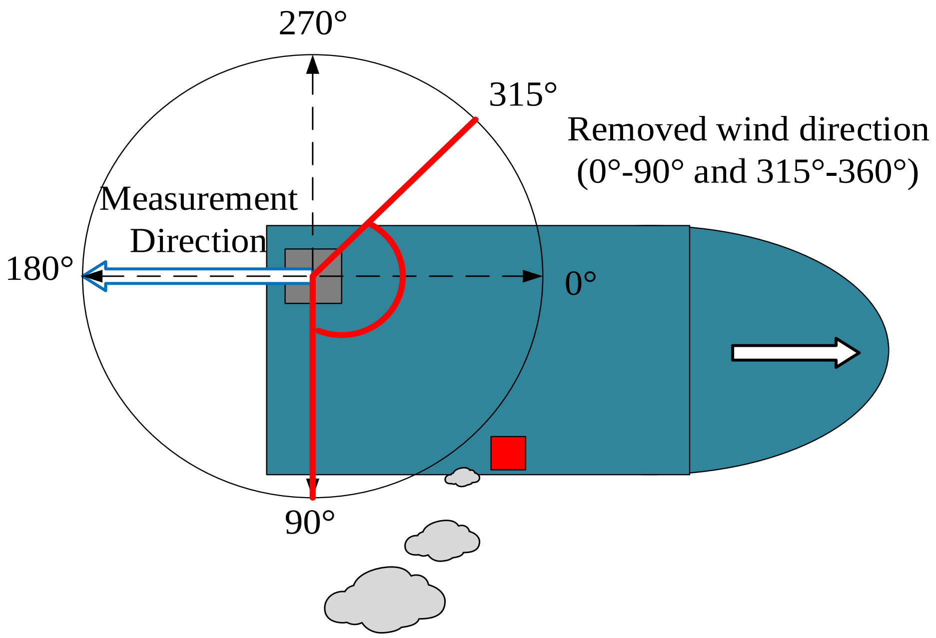

Fig. S3. Top-down schematic of the Xuelong-2 research vessel (0°denotes the direction of travel): red rectangles mark the chimney location, and gray rectangles denote the MAX-DOAS installation position.

Table S1. MAX-DOAS retrievals uncertainty

Error sources	Estimated Uncertainty
Smoothing and Noise Error	5%-10%
Uncertainty of the reference spectrum	10%-15%
Algorithm Error	10% - 20%
Errors from Stratospheric Gradient and Atmospheric Inhomogeneity	10%

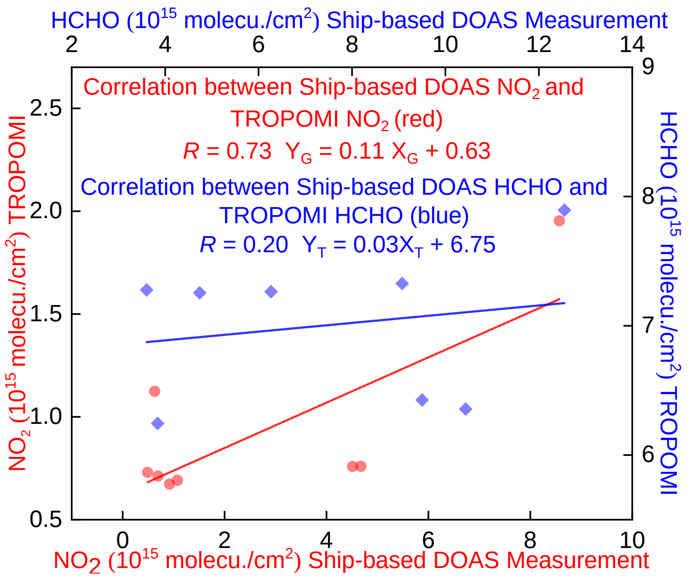

Fig. S4. Correlation between daily MAX-DOAS measurements and TROPOMI satellite. Data over 110°E–130°E, 20°N–45°N during ship-based measurements.

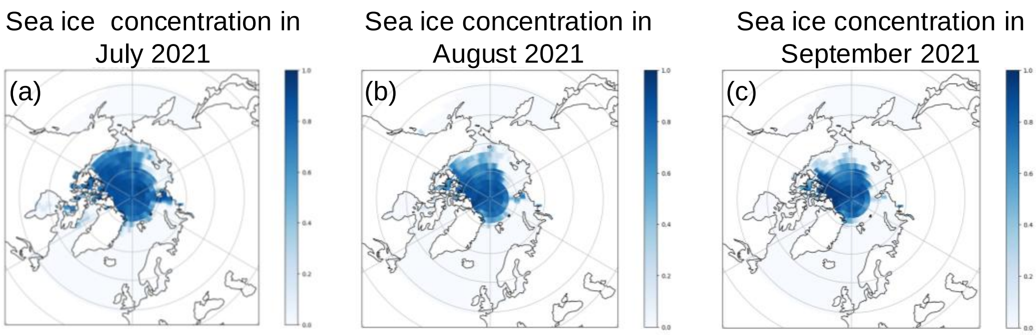

Fig. S5. Spatial distribution of Arctic sea ice concentration (July − September 2021). Data source: https://nsidc.org/home

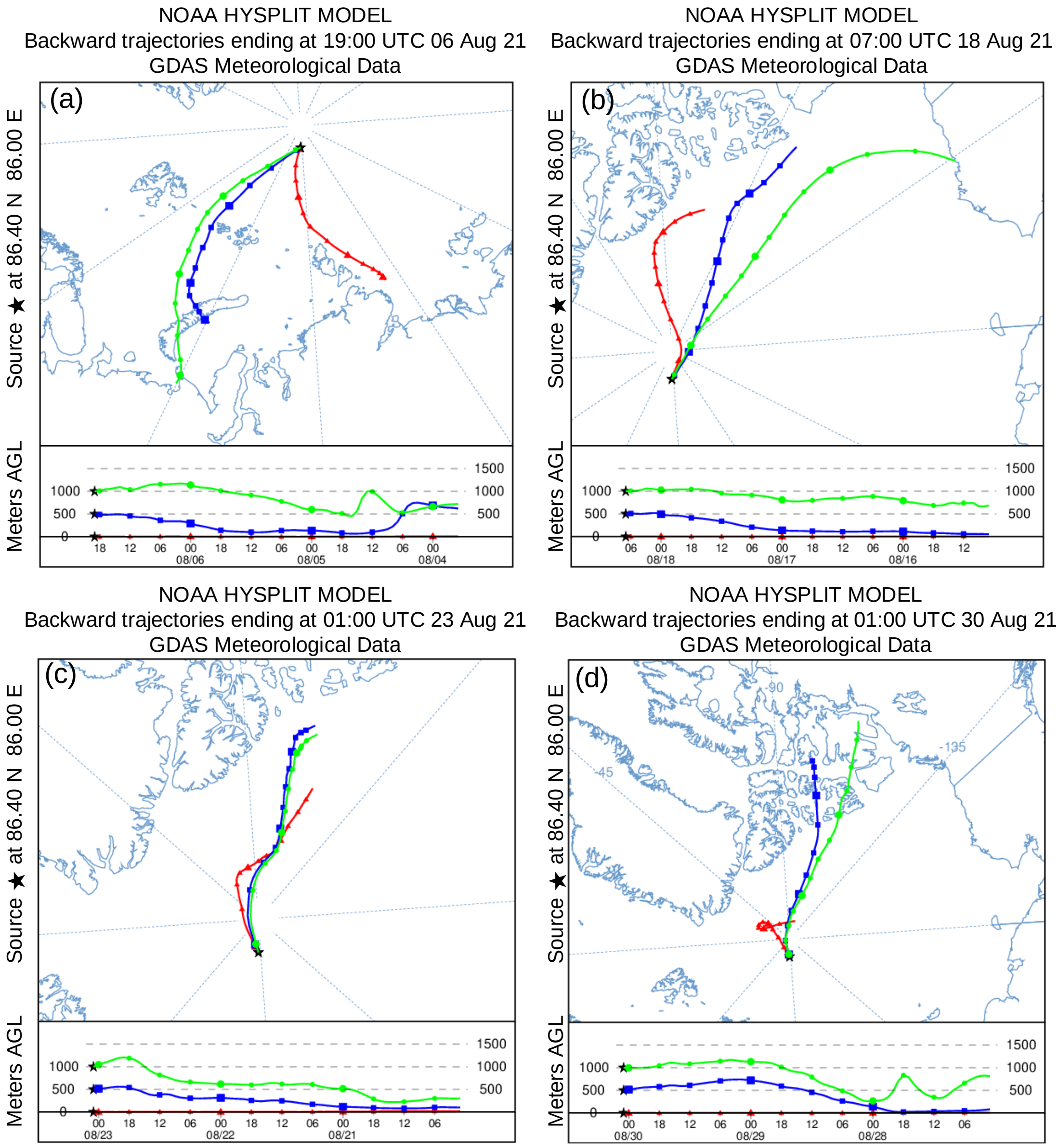

Fig. S6. Backward trajectories of polluted air masses at the target location: (a) 6 August, (b) 18 August, (c) 23 August, (d) 30 August. Curves denote trajectories originating at different altitudes:

0 m (red), 500 m (blue), 1000 m (green).

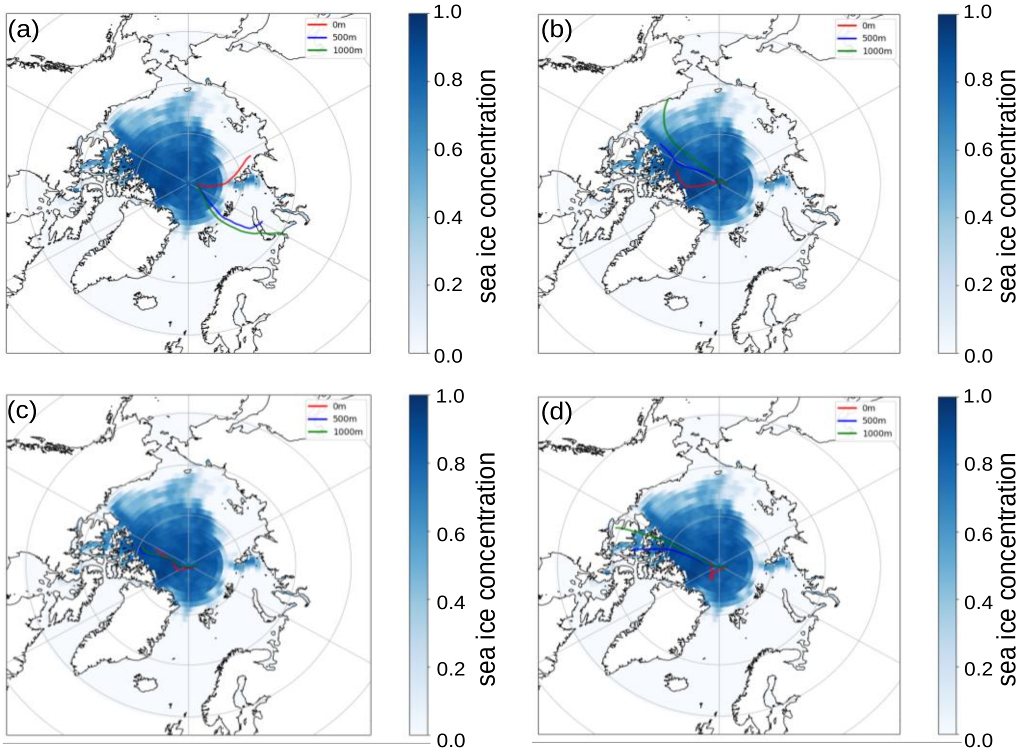

Fig. S7. Backward trajectories of polluted air masses at the target site overlaid on Arctic sea-ice concentration (August 2021)

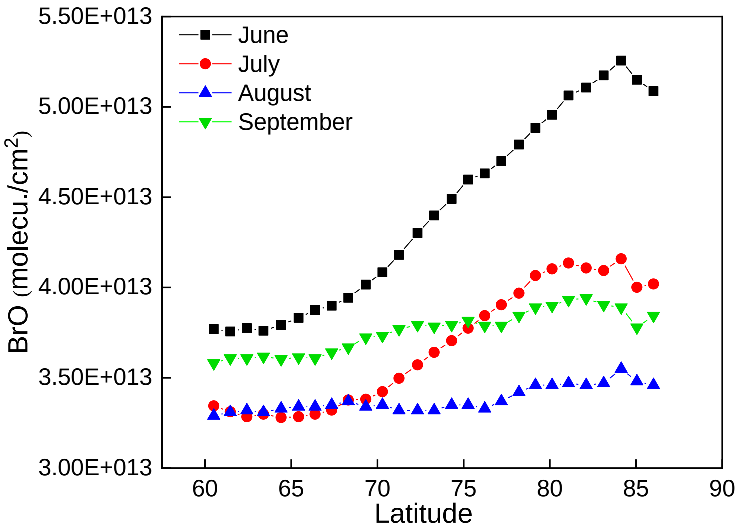

Fig. S8. BrO VCD variation from GOME-2 satellite data (July-September 2021) as a function of latitude.

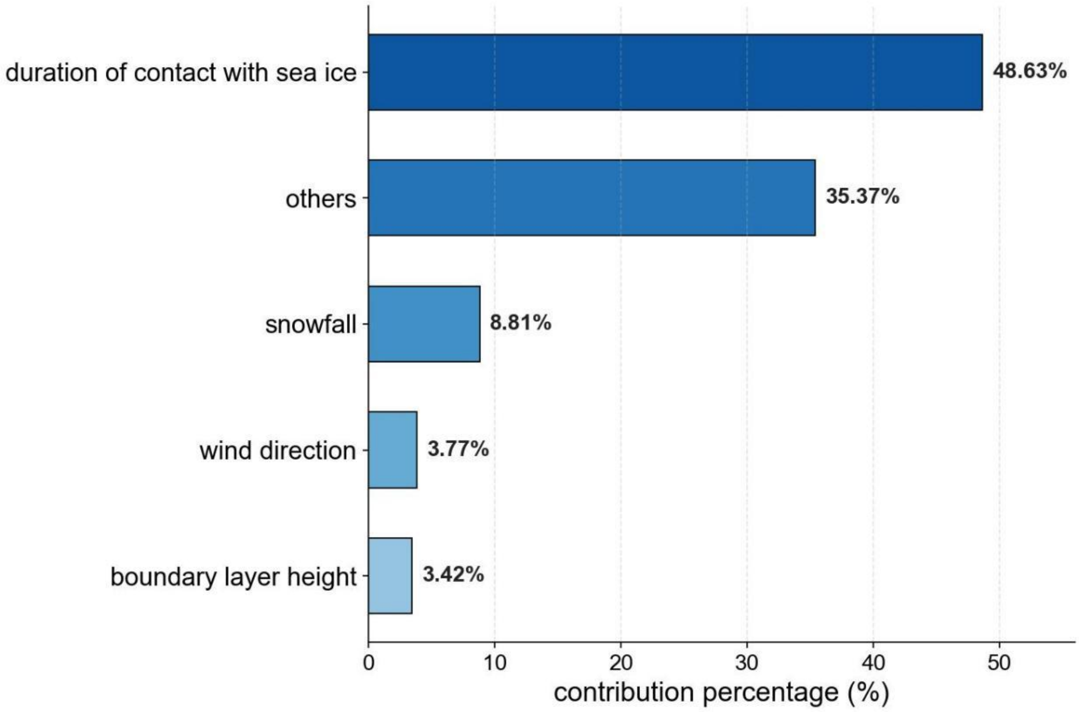

Fig. S9. Quantitative assessment of factors influencing BrO enhancement based on the generalized additive model.

To refine the quantification of material exchange between air masses and surface sources, we incorporated the boundary layer height (BLH) as a dynamic constraint for calculating sea-ice contact time. Utilizing ECMWF data for August 2021 (see Fig. S10), we coupled spatio-temporally synchronized BLH values with air mass backward trajectories. Specifically, a trajectory point was categorized as "effective sea-ice contact" only if its altitude simultaneously satisfied two conditions: being below 200 m and below the real-time BLH. This dual criterion ensures that contact occurs within the mixed layer, where surface-released reactive bromine can physically interact with the air mass via turbulent transport.

Following the integration of the BLH constraint, the correlation between tropospheric BrO concentrations and sea-ice contact time improved significantly to 0.77 (see Fig. S11). This enhancement stems from two primary factors. First, MAX-DOAS instruments typically exhibit peak vertical sensitivity within the middle and upper boundary layer (Frieß et al., 2011; Peterson et al., 2017; Simpson et al., 2017; Wagner et al., 2007). Consequently, surface emissions must undergo effective vertical mixing to reach these altitudes and be detected by the instrument. Second, the BLH serves as a physical barrier to vertical transport. If a backward trajectory's altitude exceeds the local BLH, the upward flux of reactive bromine is blocked, preventing its entrainment into the air mass. In such instances, contact with sea ice does not contribute to the observed BrO enhancements (Frieß et al., 2011; Peterson et al., 2017; Simpson et al., 2017; Wagner et al., 2007).

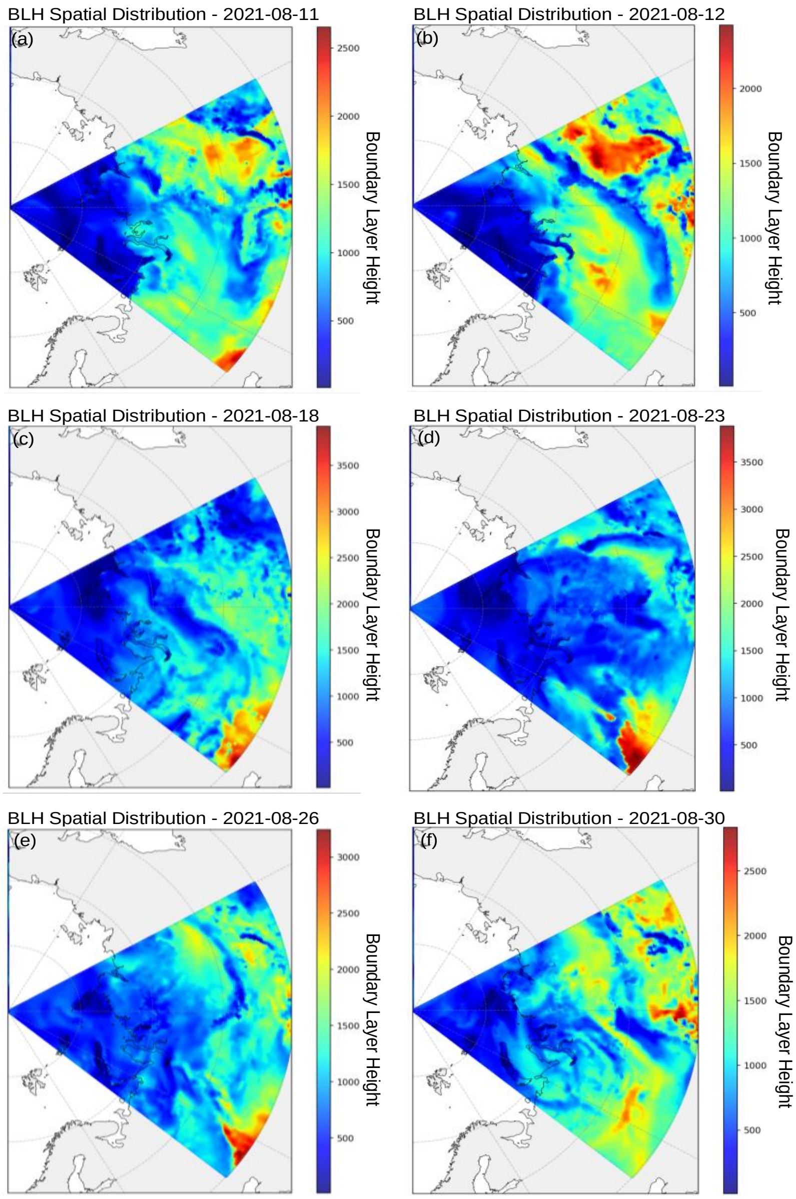

Fig. S10. Spatial distribution of boundary layer height (BLH) in the Arctic during August 2021.

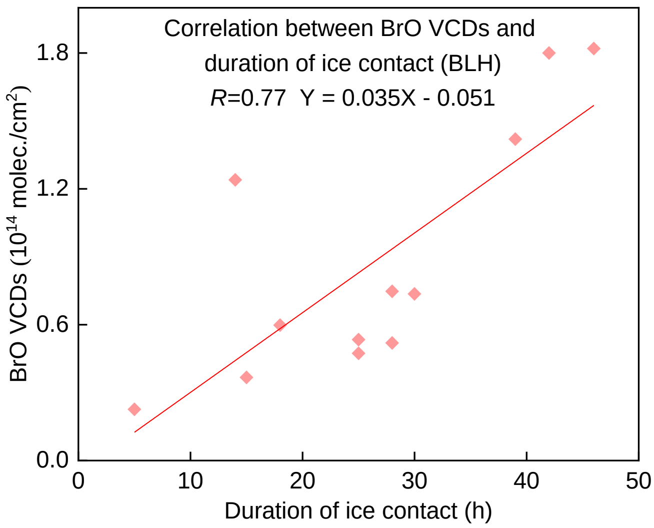

Fig. S11. Correlation analysis between tropospheric BrO concentration and sea ice contact time under boundary layer height (BLH) constraint.

Our study identifies a significant modulating role of wind direction on BrO variability. Utilizing ECMWF datasets, we analyzed the spatial distribution of Arctic wind directions for August 2021 (see Fig. S12). The findings reveal that the study area was predominantly influenced by southwesterly (SW) and southeasterly (SE) wind regimes. Under SW flow, the correlation coefficient (R) between BrO and sea-ice contact time reached 0.84, whereas SE conditions exhibited a weaker correlation of 0.65 (see Fig. S13). This spatial heterogeneity reflects how air mass trajectories dictate specific bromine activation mechanisms. The robust correlation under SW winds likely stems from airflows originating from high-salinity first-year ice (FYI) zones. These pathways are relatively stable and primarily governed by heterogeneous release from ice surfaces (Bognar et al., 2020; Brockway et al., 2024; Seo et al., 2020). In contrast, the reduced correlation under SE winds suggests that air masses encounter more complex physicochemical interference during transport (Bognar et al., 2020; Brockway et al., 2024; Seo et al., 2020). For instance, Bognar et al. (2020) observed at the Eureka station that cyclonic activity and intense atmospheric disturbances can shift BrO sources toward heterogeneous recycling on sea-salt aerosol surfaces, decoupling the concentrations from simple surface contact processes.

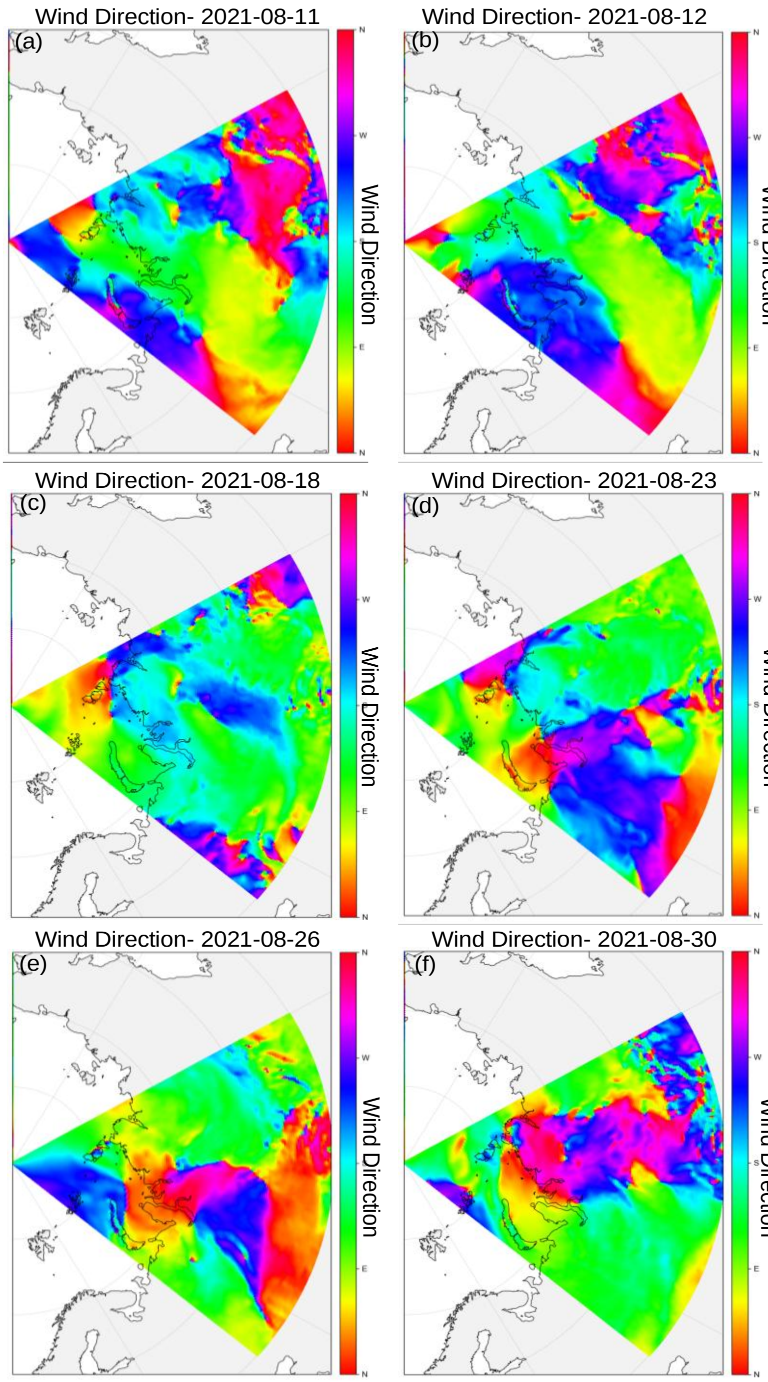

Fig. S12. Spatial distribution of wind direction in the Arctic during August 2021.

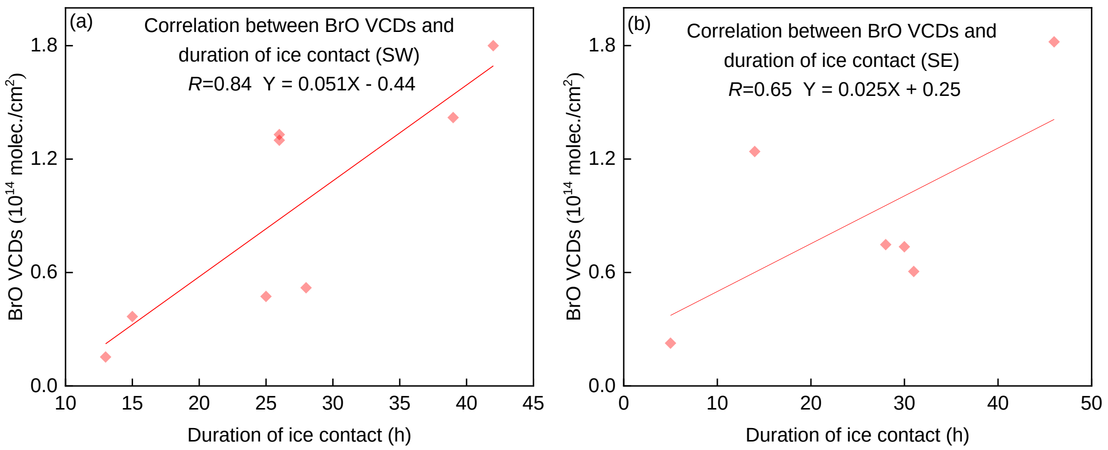

Fig. S13. Correlation analysis between tropospheric BrO concentration and sea ice contact time under wind direction constraint. (a) southwest wind direction, (b) southeast wind direction

To further explore the drivers of BrO activation, we incorporated spatial data on sea ice age (sourced from daacdata.apps.nsidc.org). Analysis for the period from July 31 to September 3, 2021, reveals that the sea ice along the cruise track and within the air mass backward trajectories consisted predominantly of first-year ice (FYI, age ≤ 1), as illustrated in Fig. S14.

Sea ice age significantly modulates the heterogeneous release of bromine, as younger ice typically exhibits higher surface salinity than multi-year ice (MYI) due to the process of brine expulsion (Bognar et al., 2020; Frieß et al., 2004; Simpson et al., 2007). Notably, Simpson et al. (2007) demonstrated that contact duration with FYI is a more reliable predictor of atmospheric BrO levels than contact with potential frost flowers. Similarly, Frieß et al. (2004) excluded MYI from their Antarctic study because its low salinity was insufficient to sustain effective bromine activation. The robust correlation (R = 0.73) observed between BrO and sea-ice contact time in this study aligns with these previous reports. Since the sampled air masses primarily interacted with high-salinity FYI, the abundant supply of bromide ions facilitated the "bromine explosion" mechanism, establishing sea-ice contact time as the primary driver of the observed BrO variability.

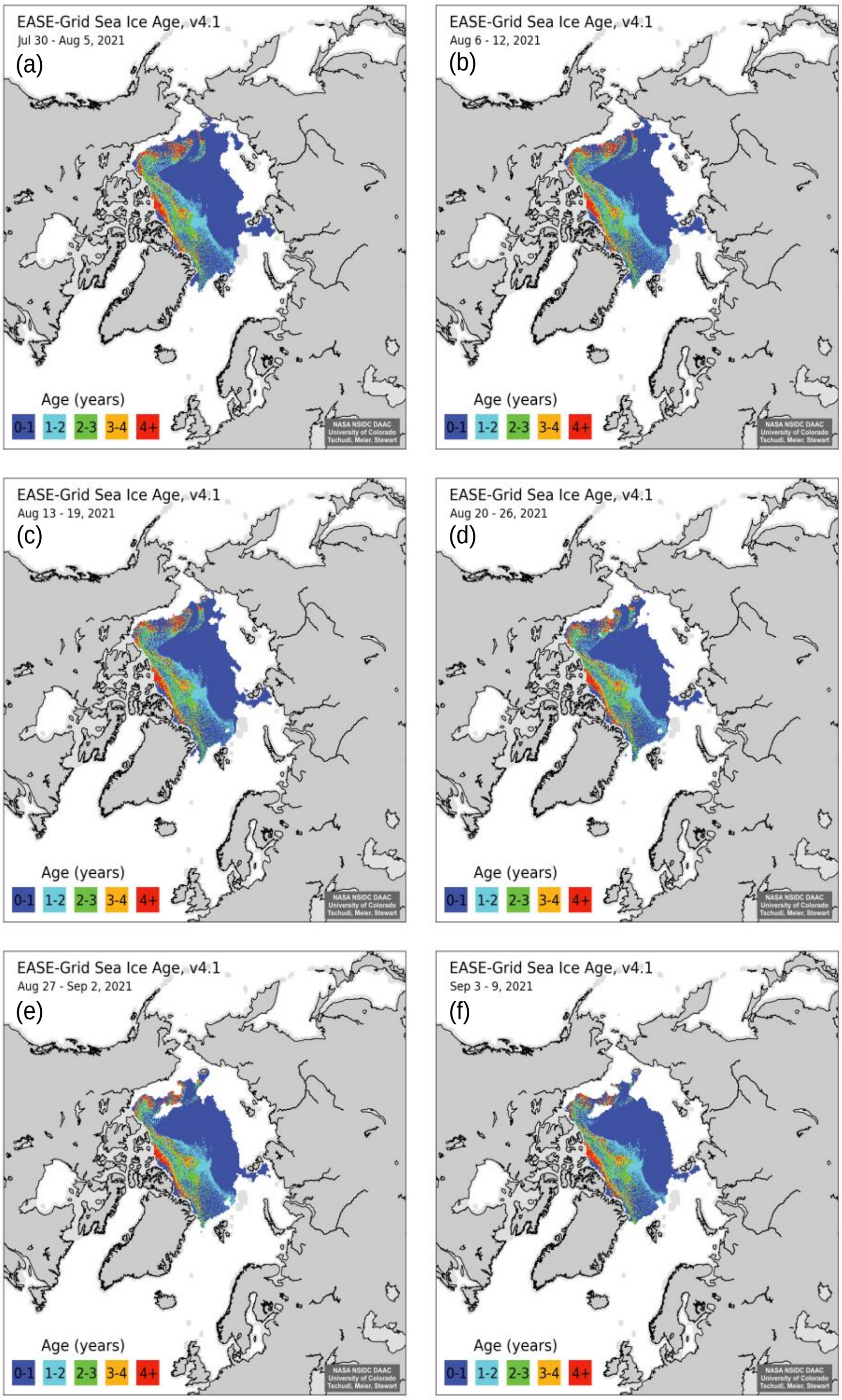

Fig. S14. Correlation analysis between tropospheric BrO concentration and sea ice contact time under sea ice age constraint. (Data source: daacdata.apps.nsidc.org)

Snowpack density is a fundamental physical parameter that determines porosity and permeability, thereby influencing brine migration from the sea-ice interface to the snow surface and the overall efficiency of heterogeneous reactions (Abbatt et al., 2012; Domine et al., 2008). In this study, we characterized the spatial distribution of snow density across the survey region using ECMWF data (see Fig. S15). By integrating geographical coordinates with air mass backward trajectories, we observed that snow density remained remarkably stable throughout the study area.

Fluctuations were negligible, staying below 1.0×10^{-5} around a mean value of 100.0 kg/m^3. Such spatial homogeneity suggests that the physical structure of the snowpack provided a consistent contribution to bromine activation along all sampled trajectory paths.

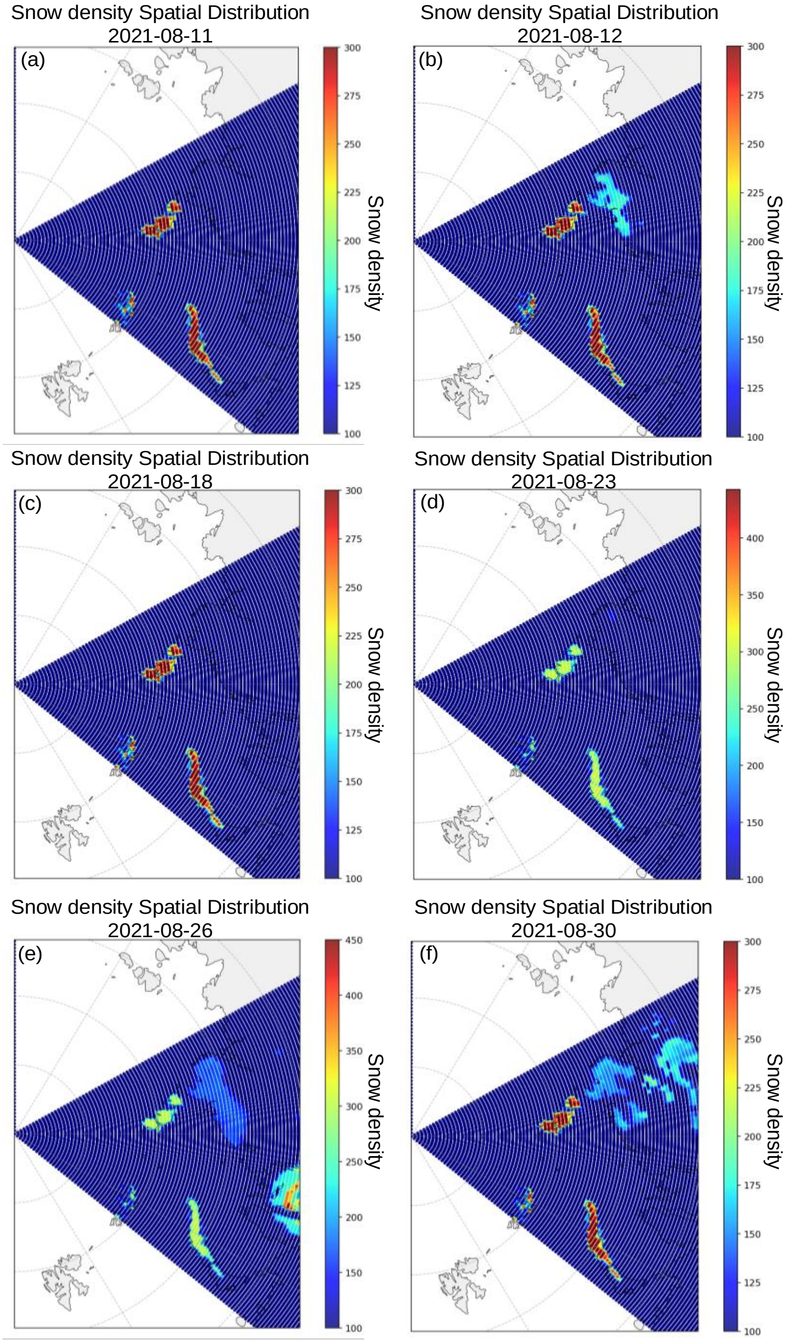

Fig. S15. Correlation analysis between tropospheric BrO concentration and sea ice contact time under snow density constraint.

As a critical meteorological forcing that alters polar surface characteristics and atmospheric loading (Bognar et al., 2020; Burd et al., 2017; Frey et al., 2020; Peterson et al., 2017; Pratt et al., 2013), snowfall significantly modulates BrO variability. In this study, we analyzed the spatial distribution of Arctic snowfall for August 2021 based on ECMWF data (see Fig. S16). To evaluate the modulating role of snowfall, we partitioned the observations into snow-free (snowfall = 0) and active snowfall (snowfall > 0) periods.

Our analysis indicates that while a robust correlation (R = 0.87) exists under snow-free conditions, this relationship weakens to R = 0.61 during snowfall events (see Fig. S17). Several mechanisms likely drive this divergence. Initially, the accumulation of fresh snow can physically mask bromine-rich substrates, such as saline snowpacks on first-year ice or frost flowers, which suppresses the heterogeneous release of reactive bromine into the atmosphere (Bognar et al., 2020; Burd et al., 2017; Frey et al., 2020; Peterson et al., 2017; Pratt et al., 2013). Additionally, wet deposition during snowfall efficiently removes reactive bromine species and recycling aerosols from the air, decoupling BrO concentrations from simple sea-ice contact durations (Bognar et al., 2020; Burd et al., 2017; Frey et al., 2020; Peterson et al., 2017; Pratt et al., 2013). Finally, as noted by Bognar et al. (2020), snowfall in the Arctic is frequently coupled with cyclonic activity. The resulting high winds and boundary layer instabilities trigger vigorous vertical mixing, shifting BrO variability from a regime dominated by surface contact to one governed by complex, nonlinear multivariable dynamics.

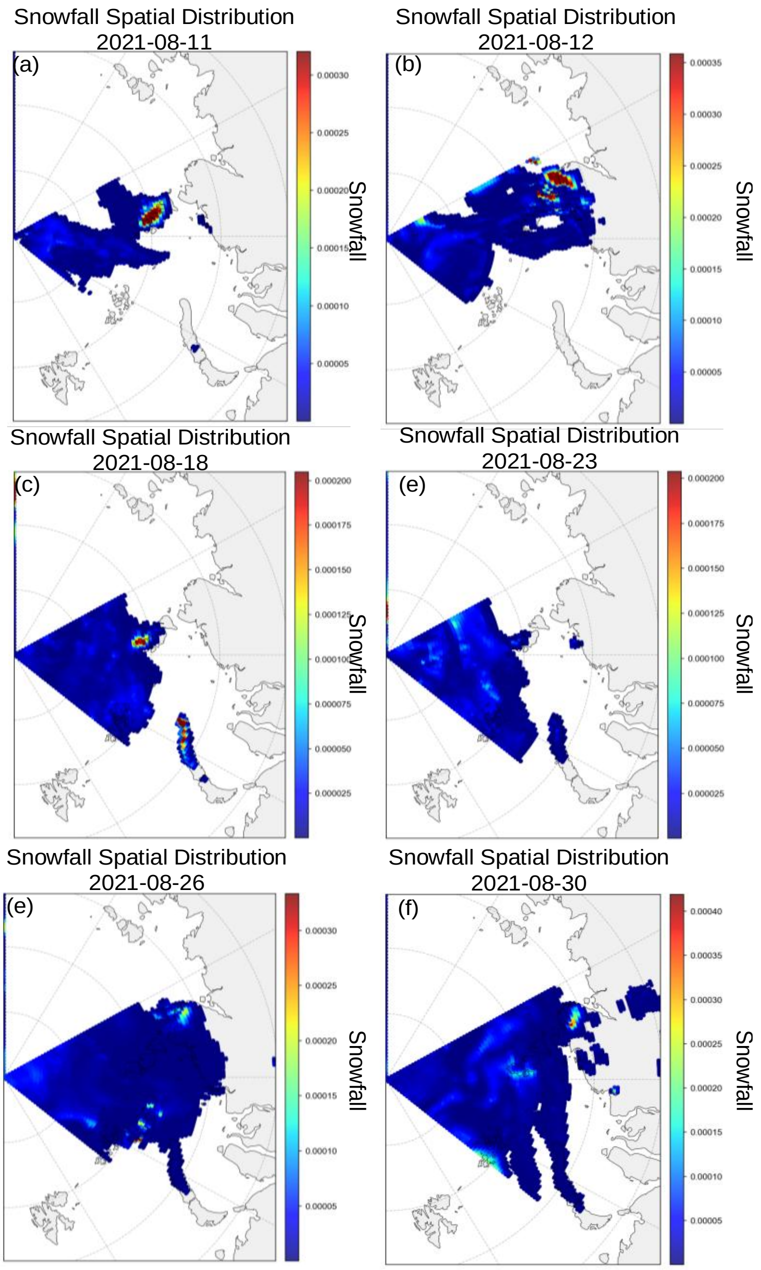

Fig. S16. Correlation analysis between tropospheric BrO concentration and sea ice contact time under snowfall constraint.

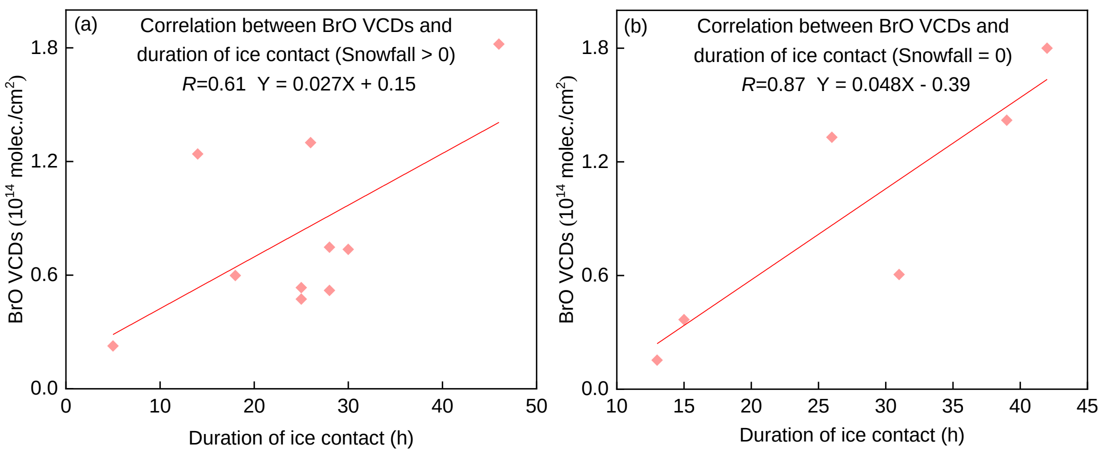

Fig. S17. Correlation analysis between tropospheric BrO concentration and sea ice contact time under snowfall. (a) snowfall > 0, (b)snowfall = 0.

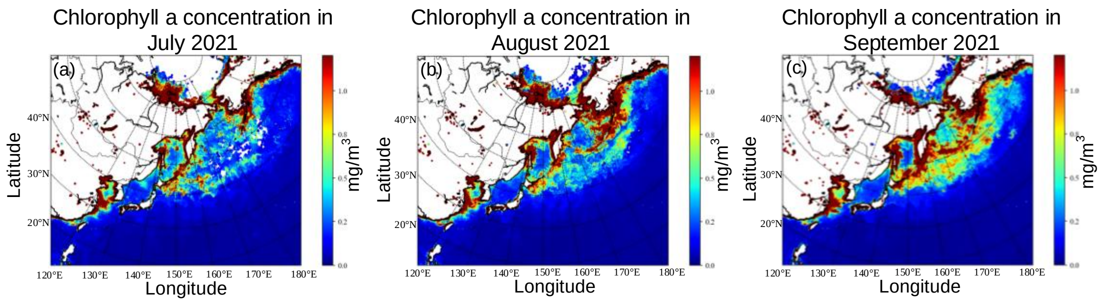

Fig. S18. Spatial distribution of chlorophyll a concentration (July-September 2021). Data source: https://aqua.nasa.gov/modis

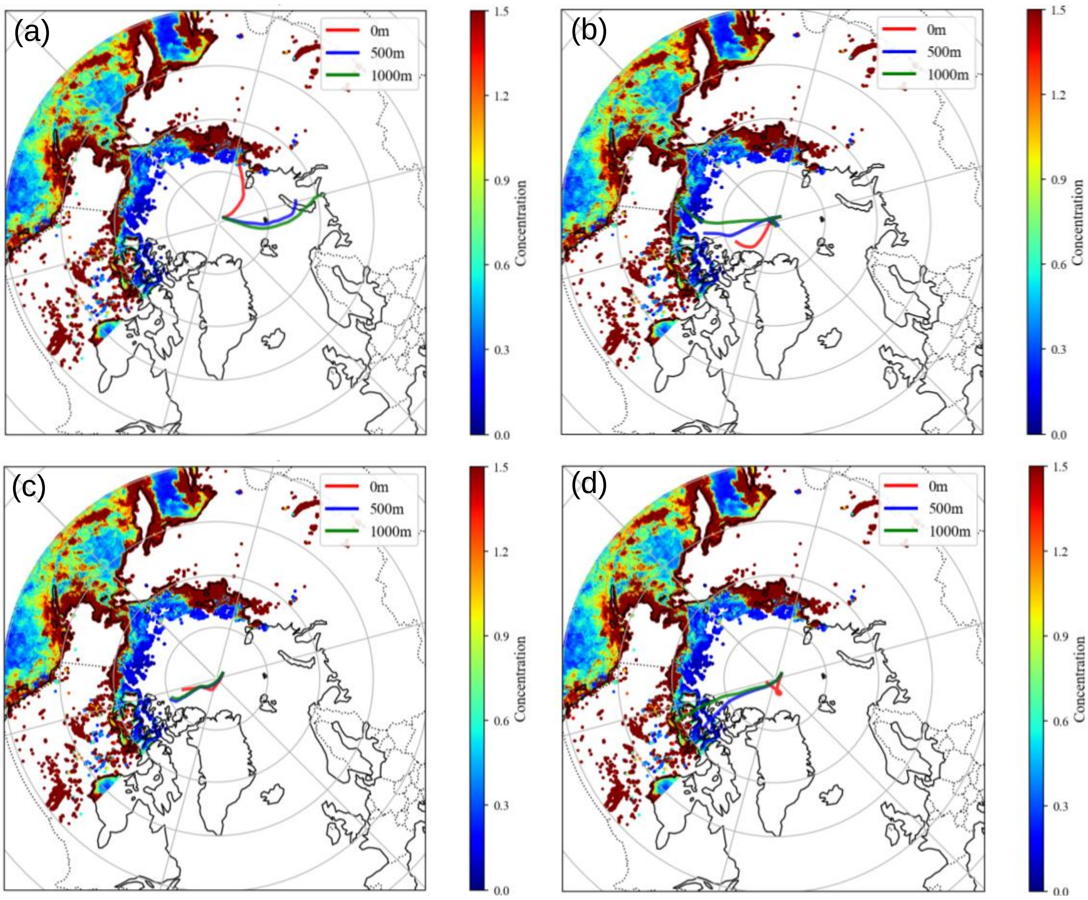

Fig. S19. Backward trajectories of polluted air masses at the target location over Arctic chlorophyll-a concentration (August 2021)

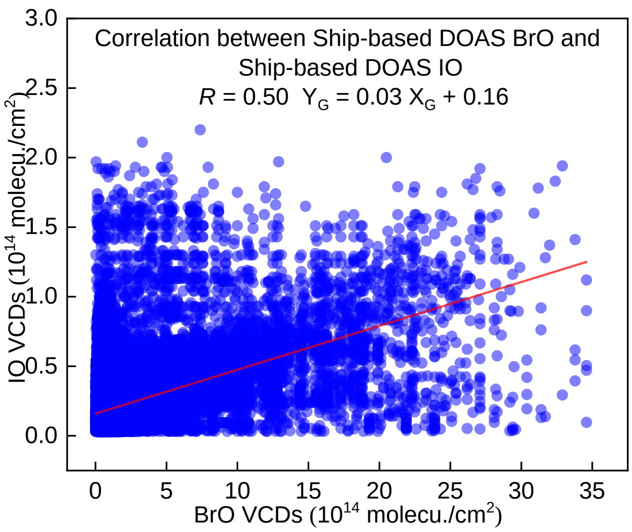

Fig. S20. Correlation between ship-based MAX-DOAS BrO VCDs and IO VCDs

Reference

Abbatt, J. P. D., Thomas, J. L., Abrahamsson, K., Boxe, C., Granfors, A., Jones, A. E., King, M. D., Saiz-Lopez, A., Shepson, P. B., Sodeau, J., Toohey, D. W., Toubin, C., von Glasow, R., Wren, S. N., and Yang, X.: Halogen activation via interactions with environmental ice and snow in the polar lower troposphere and other regions, Atmospheric Chemistry and Physics, 12, 6237–6271, https://doi.org/10.5194/acp-12-6237-2012, 2012.

Bognar, K., Zhao, X., Strong, K., Chang, R. Y. W., Frieß, U., Hayes, P. L., McClure-Begley, A., Morris, S., Tremblay, S., and Vicente-Luis, A.: Measurements of Tropospheric Bromine Monoxide Over Four Halogen Activation Seasons in the Canadian High Arctic, Journal of Geophysical Research: Atmospheres, 125, e2020JD033015, https://doi.org/10.1029/2020JD033015, 2020.

Brockway, N., Peterson, P. K., Bigge, K., Hajny, K. D., Shepson, P. B., Pratt, K. A., Fuentes, J. D., Starn, T., Kaeser, R., Stirm, B. H., and Simpson, W. R.: Tropospheric bromine monoxide vertical profiles retrieved across the Alaskan Arctic in springtime, Atmospheric Chemistry and Physics, 24, 23–40, https://doi.org/10.5194/acp-24-23-2024, 2024.

Burd, J. A., Peterson, P. K., Nghiem, S. V., Perovich, D. K., and Simpson, W. R.: Snowmelt onset hinders bromine monoxide heterogeneous recycling in the Arctic, Journal of Geophysical Research: Atmospheres, 122, 8297–8309, https://doi.org/10.1002/2017JD026906, 2017.

Domine, F., Albert, M., Huthwelker, T., Jacobi, H.-W., Kokhanovsky, A. A., Lehning, M., Picard, G., and Simpson, W. R.: Snow physics as relevant to snow photochemistry, Atmospheric Chemistry and Physics, 8, 171–208, https://doi.org/10.5194/acp-8-171-2008, 2008.

Frey, M. M., Norris, S. J., Brooks, I. M., Anderson, P. S., Nishimura, K., Yang, X., Jones, A. E., Nerentorp Mastromonaco, M. G., Jones, D. H., and Wolff, E. W.: First direct observation of sea salt aerosol production from blowing snow above sea ice, Atmospheric Chemistry and Physics, 20, 2549–2578, https://doi.org/10.5194/acp-20-2549-2020, 2020.

Frieß, U., Hollwedel, J., König-Langlo, G., Wagner, T., and Platt, U.: Dynamics and chemistry of tropospheric bromine explosion events in the Antarctic coastal region, Journal of Geophysical Research: Atmospheres, 109, https://doi.org/10.1029/2003JD004133, 2004.

Frieß, U., Sihler, H., Sander, R., Pöhler, D., Yilmaz, S., and Platt, U.: The vertical distribution of

BrO and aerosols in the Arctic: Measurements by active and passive differential optical absorption spectroscopy, Journal of Geophysical Research: Atmospheres, 116, https://doi.org/10.1029/2011JD015938, 2011.

Peterson, P. K., Pöhler, D., Sihler, H., Zielcke, J., General, S., Frieß, U., Platt, U., Simpson, W. R., Nghiem, S. V., Shepson, P. B., Stirm, B. H., Dhaniyala, S., Wagner, T., Caulton, D. R., Fuentes, J. D., and Pratt, K. A.: Observations of bromine monoxide transport in the Arctic sustained on aerosol particles, Atmospheric Chemistry and Physics, 17, 7567–7579, https://doi.org/10.5194/acp-17-7567-2017, 2017.

Pratt, K. A., Custard, K. D., Shepson, P. B., Douglas, T. A., Pöhler, D., General, S., Zielcke, J., Simpson, W. R., Platt, U., Tanner, D. J., Gregory Huey, L., Carlsen, M., and Stirm, B. H.: Photochemical production of molecular bromine in Arctic surface snowpacks, Nature Geoscience, 6, 351–356, https://doi.org/10.1038/ngeo1779, 2013.

Seo, S., Richter, A., Blechschmidt, A.-M., Bougoudis, I., and Burrows, J. P.: Spatial distribution of enhanced BrO and its relation to meteorological parameters in Arctic and Antarctic sea-ice regions, Atmospheric Chemistry and Physics, 20, 12285–12312, https://doi.org/10.5194/acp-20-12285-2020, 2020.

Simpson, W. R., Carlson, D., Hönninger, G., Douglas, T. A., Sturm, M., Perovich, D., and Platt, U.: First-year sea-ice contact predicts bromine monoxide (BrO) levels at Barrow, Alaska better than potential frost flower contact, Atmospheric Chemistry and Physics, 7, 621–627, https://doi.org/10.5194/acp-7-621-2007, 2007.

Simpson, W. R., Peterson, P. K., Frieß, U., Sihler, H., Lampel, J., Platt, U., Moore, C., Pratt, K., Shepson, P., Halfacre, J., and Nghiem, S. V.: Horizontal and vertical structure of reactive bromine events probed by bromine monoxide MAX-DOAS, Atmospheric Chemistry and Physics, 17, 9291–9309, https://doi.org/10.5194/acp-17-9291-2017, 2017.

Wagner, T., Ibrahim, O., Sinreich, R., Frieß, U., von Glasow, R., and Platt, U.: Enhanced tropospheric BrO over Antarctic sea-ice in mid-winter observed by MAX-DOAS on board the research vessel Polarstern, Atmospheric Chemistry and Physics, 7, 3129–3142, https://doi.org/10.5194/acp-7-3129-2007, 2007.